INTERNATIONAL CONGRESS ON
FLUID DYNAMICS & PROPULSION
DECEMBER 29-31,1996 CAIRO, EGYPT

C/5 138

INHOMOGENEOUS RADIATION BOUNDARY CONDITIONS SIMULATING INCOMING ACOUSTIC WAVES FOR COMPUTATIONAL AEROACOUSTICS

Christopher K.W. Tam, Jun Fang and Konstantin A. Kurbatskii
Department of Mathematics
Florida State University
Tallahassee, FL 32306-3027, USA

ABSTRACT

A set of nonhomogeneous radiation and outflow boundary conditions which automatically generate prescribed incoming acoustic or vorticity waves and, at the same time, are transparent to outgoing sound waves produced internally in a finite computation domain is proposed. This type of boundary condition is needed for the numerical solution of many exterior aeroacoustics problems. In computational aeroacoustics, the computation scheme must be as nondispersive and nondissipative as possible. It must also support waves with wave speeds which are nearly the same as those of the original linearized Euler equations. To meet these requirements, a high-order/large-stencil scheme is necessary. The proposed nonhomogeneous radiation and outflow boundary conditions are designed primarily for use in conjunction with such high-order/large-stencil finite difference schemes.

1. INTRODUCTION

Many exterior aeroacoustics problems involve incoming acoustic or vorticity waves interacting with an aircraft engine or the body of the aircraft. An example of this type of problem that is of current interest is the noise generation by the ingestion of free stream turbulence into a fan engine. Another example is the scattering and shielding of sound waves by aircraft wings and fuselage. To simulate these problems using computational aeroacoustics methods, the incoming acoustic and vorticity waves must be generated by the boundary conditions imposed at the outer boundaries of the finite computation domain. In this paper, a set of nonhomogeneous radiation and outflow boundary conditions, which, when used in conjunction with a high-order finite difference scheme, automatically generates the desired incoming acoustic and vorticity waves is proposed.

In the presence of a uniform mean flow, the linearized Euler equations support three independent types of small amplitude disturbances. They are the acoustic, the vorticity and the entropy waves. These waves, to linear order, are uncoupled and propagate with different characteristics and wave speeds (see e.g., Tam and Webb (1993)). In the computational aeroacoustics literature, there seems to be an absence of suggestions as to how to generate such disturbances in the form of incoming waves. There are two intrinsic difficulties. First, the imposed boundary conditions must not only generate the prescribed incoming waves, they must also be transparent to outgoing acoustic disturbances produced inside the computation domain. Second, because the Euler equations support both acoustic and vorticity waves at the same spatial location, it is extremely difficult to generate a single type of disturbance without also producing the other type. Such coupling usually occurs at the corner regions of the computation domain. The proposed nonhomogeneous radiation and outflow boundary conditions are designed specifically to overcome these difficulties.

In this work, we will use the Dispersion-Relation-Preserving (DRP) scheme of Tam and Webb (1993) for numerical computation. There are two reasons for choosing the DRP scheme. First, the DRP scheme was designed so that the dispersion relations of the finite difference equations are always formally identical to those of the original partial differential equations. This not only makes the waves supported by the numerical scheme an excellent approximation of those of the partial differential equations, it also assures that there will be no wave mode coupling in the numerical simulation. The second reason for choosing the DRP scheme is that the exact plane acoustic, vorticity and entropy wave solutions of the finite difference equations can be found analyt-

ically. This is discussed in Section 2 of this paper. These exact solutions are used in formulating the nonhomogeneous radiation and outflow boundary conditions.

Over the years, there has been a number of investigations devoted to the development of radiation/nonreflecting boundary conditions but without incoming waves. Recently, Hixon, Shih and Mankbadi (1995) performed a detailed evaluation of the suitability of using the Thompson (1987, 1990) quasi-one-dimensional characteristic boundary condition, the Giles (1990) Fourier mode decomposition boundary treatment and the asymptotic boundary conditions of Tam and Webb (1993) for computational aeroacoustics applications. They concluded that for their test problem, the radiation and outflow boundary conditions of Tam and Webb gave the least reflections and provided the only acceptable boundary treatment. In this work, we follow their recommendation and use the asymptotic boundary conditions of Tam and Webb to develop the nonhomogeneous radiation and outflow boundary conditions that would automatically produce very accurate incoming acoustic and vorticity waves in a finite computation domain.

2. ACOUSTIC AND VORTICITY WAVES ON A GRID

We will consider small amplitude disturbances superimposed on a uniform mean flow of Mach number M as shown in Figure 1. Such disturbances are governed by the linearized Euler equations. We will use dimensionless variables with length scale = Δx = Δy (the mesh spacing), velocity scale = a_0 (speed of sound), time scale = $\frac{\Delta x}{a_0}$, pressure scale = $\rho_0 a_0^2$ (where ρ_0 is the gas density). The dimensionless linearized Euler equations are

$$\frac{\partial \mathsf{F}}{\partial t} + \mathsf{R}\frac{\partial \mathsf{F}}{\partial x} + \mathsf{S}\frac{\partial \mathsf{F}}{\partial y} = 0 \qquad (2.1)$$

where F, the solution vector, and matrices R and S are

$$\mathsf{F} = \begin{bmatrix} u \\ v \\ p \end{bmatrix}, \quad \mathsf{R} = \begin{bmatrix} M_x & 0 & 1 \\ 0 & M_x & 0 \\ 1 & 0 & M_x \end{bmatrix}, \quad \mathsf{S} = \begin{bmatrix} M_y & 0 & 0 \\ 0 & M_y & 1 \\ 0 & 1 & M_y \end{bmatrix}. \qquad (2.2)$$

In (2.2) M_x and M_y are the mean flow Mach numbers in the x- and y-directions. If ϕ is the direction of the mean flow measured from the x-axis, then $M_x = M\cos\phi$, $M_y = M\sin\phi$.

Upon discretizing (2.1) according to the DRP scheme, the finite difference equations may be written in the following form

$$\mathsf{F}_{\ell,m}^{(n+1)} = \mathsf{F}_{\ell,m}^{(n)} + \Delta t \sum_{j=0}^{3} b_j \, \mathsf{K}_{\ell,m}^{(n-j)}. \qquad (2.3)$$

Subscripts (ℓ, m) are the spatial indices of the mesh in the x- and y-directions. Superscript n is the time level. Δt is the time step. The vector $\mathsf{K}_{\ell,m}^{(n)}$ is given by

$$\mathsf{K}_{\ell,m}^{(n)} = -\mathsf{R}\sum_{j=-3}^{3} a_j \, \mathsf{F}_{\ell+j,m}^{(n)} - \mathsf{S}\sum_{j=-3}^{3} a_j \, \mathsf{F}_{\ell,m+j}^{(n)} - \frac{1}{R_{\Delta x}}\sum_{j=-3}^{3} d_j \left(\mathsf{F}_{\ell+j,m}^{(n)} + \mathsf{F}_{\ell,m+j}^{(n)}\right). \qquad (2.4)$$

The last sum on the right side of (2.4) is the artificial damping terms. $R_{\Delta x}$ is the mesh Reynolds number. The numerical values of the stencil coefficients a_j, b_j and d_j may be found in Tam (1995).

We will look for plane wave solutions of finite difference equations (2.3) and (2.4) over an infinite mesh. The analytical form of the finite difference solution is

$$\mathsf{F}_{\ell,m}^{(n)} = \mathrm{Re}\left\{\hat{\mathsf{F}}\, e^{i(\alpha\ell + \beta m - \omega n\Delta t)}\right\}. \qquad (2.5)$$

In (2.5), Re{ } is the real part of. $\hat{\mathsf{F}}$ is the wave amplitude vector (a constant vector). (α, β) are the wave numbers. ω is the angular frequency. Substitution of (2.5) into (2.3) and (2.4), after some algebra, the following matrix equation for $\hat{\mathsf{F}}$ is derived.

$$\mathsf{A}\,\hat{\mathsf{F}} = \mathbf{0}. \qquad (2.6)$$

The matrix A is equal to

$$\mathsf{A} = \begin{bmatrix} -\bar{\omega} & 0 & \bar{\alpha} \\ 0 & -\bar{\omega} & \bar{\beta} \\ \bar{\alpha} & \bar{\beta} & -\bar{\omega} \end{bmatrix} \tag{2.7}$$

where

$$\begin{aligned} \bar{\omega} &= \left[\bar{\omega} - M_x\bar{\alpha} - M_y\bar{\beta} + \frac{i(D(\alpha)+D(\beta))}{R_{\Delta x}}\right] \\ \bar{\alpha} &= -i\sum_{j=-3}^{3} a_j e^{ij\alpha} \\ \bar{\beta} &= -i\sum_{j=-3}^{3} a_j e^{ij\beta} \\ \bar{\omega} &= \frac{i(e^{-i\omega\Delta t}-1)}{\Delta t\sum_{j=0}^{3} b_j e^{ij\omega\Delta t}} \\ D(\alpha) &= \sum_{j=-3}^{3} d_j e^{-ij\alpha} \\ D(\beta) &= \sum_{j=-3}^{3} d_j e^{-ij\beta}. \end{aligned} \tag{2.8}$$

The quantities $(\bar{\alpha}, \bar{\beta})$ and $\bar{\omega}$ are the wavenumbers and angular frequency of the computation scheme (the DRP scheme). $D(\alpha)$ and $D(\beta)$ are the artificial selective damping functions (see Tam (1995)).

For nontrivial solution of equation (2.6), the determinant of the coefficient matrix A must be equal to zero. This condition leads to the general dispersion relation

$$\bar{\omega}(\bar{\omega}^2 - \bar{\alpha}^2 - \bar{\beta}^2) = 0. \tag{2.9}$$

We wish to point out that the Dispersion-Relation-Preserving scheme assures that dispersion relation (2.9) is the same as that of the waves of the original linearized Euler equations provided the following substitutions are made: $\bar{\omega} \to \omega$, $\bar{\alpha} \to \alpha$, $\bar{\beta} \to \beta$ and $\frac{1}{R_{\Delta x}} \to 0$.

2.1 Acoustic waves

For acoustic waves, the dispersion relation is obtained by equating the second factor of (2.9) to zero. This gives,

$$\left[\bar{\omega} - M_x\bar{\alpha} - M_y\bar{\beta} + \frac{i(D(\alpha)+D(\beta))}{R_{\Delta x}}\right]^2 - \bar{\alpha}^2 - \bar{\beta}^2 = 0. \tag{2.10}$$

The corresponding eigenvector is

$$\hat{\mathsf{F}} \equiv \begin{bmatrix} F_1 \\ F_2 \\ F_3 \end{bmatrix} = \begin{bmatrix} \bar{\alpha}/\bar{\omega} \\ \bar{\beta}/\bar{\omega} \\ 1 \end{bmatrix}. \tag{2.11}$$

Suppose the direction of propagation of the incoming plane acoustic waves is χ (measured from the x-axis) as shown in Figure 1. Here the direction of propagation is taken to be normal to the lines of constant phase. It follows, therefore, that α and β must be such that

$$\tan\chi = \frac{\beta}{\alpha}. \tag{2.12}$$

A plane acoustic wave may be characterized by its frequency ω and the direction of propagation χ. The wavenumbers (α, β) of such a wave can be found by solving equations (2.10) and (2.12) simultaneously. With the inclusion of artificial damping in the finite difference scheme, equation (2.4), the wavenumbers (α, β) of the wave are complex. Since only a small amount of damping is added, the imaginary parts are small. The wavenumbers of the corresponding acoustic wave solution of the linearized Euler equations are, however, real.

2.2 Vorticity waves

The dispersion relation for the vorticity waves of the finite difference scheme is given by setting $\bar{\omega}$ to zero in (2.9); i.e.,

$$\bar{\omega} - M_x\bar{\alpha} - M_y\bar{\beta} + \frac{i}{R_{\Delta x}}(D(\alpha) + D(\beta)) = 0. \tag{2.13}$$

The corresponding eigenfunction is

$$\hat{\mathsf{G}} \equiv \begin{bmatrix} G_1 \\ G_2 \\ 0 \end{bmatrix} = \begin{bmatrix} \frac{\bar{\beta}}{(\bar{\alpha}^2+\bar{\beta}^2)^{1/2}} \\ \frac{-\bar{\alpha}}{(\bar{\alpha}^2+\bar{\beta}^2)^{1/2}} \\ 0 \end{bmatrix}. \tag{2.14}$$

Let ψ be the angle between the lines of constant phase of the vorticity waves and the x-axis (see Figure 1) then

$$\tan\psi = -\cot\chi = -\frac{\alpha}{\beta}. \tag{2.15}$$

A vorticity wave may be specified by its frequency ω and the phase angle ψ. The wavenumbers of such waves are found by solving equations (2.13) and (2.15) simultaneously. Because of the inclusion of artificial damping terms, the wavenumbers are again complex.

3. INHOMOGENEOUS RADIATION AND OUTFLOW BOUNDARY CONDITIONS

We will now consider how to carry out numerical simulation of exterior aeroacoustics problems involving incoming acoustic or vorticity waves. By necessity, the computation domain is finite. Without loss of generality, we will consider the flow configuration to be as shown in Figure 1. With the inflow as prescribed, the bottom and the left side of the computation domain constitute the inflow boundaries. The right and top sides are the outflow boundaries.

In the absence of incoming waves, the radiation boundary conditions of Tam and Web (1993) may be imposed along the inflow boundaries. In polar coordinates (r,θ) with origin at the center of the computation domain, these radiation boundary conditions for the outgoing waves, F_{out}, may be written as,

$$\frac{\partial \mathsf{F}_{\text{out}}}{\partial t} = -V(\theta)\left(\frac{\partial}{\partial r} + \frac{1}{2r}\right)\mathsf{F}_{\text{out}}. \tag{3.1}$$

The acoustic wave propagation velocity $V(\theta)$ of (3.1) is equal to,

$$V(\theta) = M\cos(\theta-\phi) + [1 - M^2\sin^2(\theta-\phi)]^{\frac{1}{2}}. \tag{3.2}$$

Along the outflow boundaries, Tam and Webb showed that the outgoing disturbances may be comprised of acoustic, vorticity and entropy waves. By means of the asymptotic solutions of these waves, they demonstrated that for pressure, p_{out}, the outflow boundary condition is the same as (3.1). For the velocity components, $(u_{\text{out}}, v_{\text{out}})$, the approximate outflow boundary conditions are,

$$\frac{\partial}{\partial t}\begin{bmatrix} u_{\text{out}} \\ v_{\text{out}} \end{bmatrix} = -\left[M_x\frac{\partial}{\partial x} + M_y\frac{\partial}{\partial y}\right]\cdot\begin{bmatrix} u_{\text{out}} \\ v_{\text{out}} \end{bmatrix} - \begin{bmatrix} \frac{\partial}{\partial x} \\ \frac{\partial}{\partial y} \end{bmatrix} p_{\text{out}}. \tag{3.3}$$

3.1 Incoming acoustic waves

As discussed in Section 2, an incoming plane acoustic wave on a grid has a mathematical solution in the form

$$\begin{bmatrix} u \\ v \\ p \end{bmatrix}_{\ell,m}^{(n)} \equiv \mathsf{F} = \text{Re}\left\{\hat{\mathsf{F}}\, e^{i(\alpha\ell+\beta m-\omega n\Delta t)}\right\} \tag{3.4}$$

where $\hat{\mathsf{F}}$, the eigenvector, is given by (2.11) and the wavenumbers (α,β) are to be found by solving equations (2.10) and (2.12) simultaneously. Let $\mathsf{F}_{\ell,m}^{(n)}$ be the numerical solution of the discretized linearized Euler equations. At the inflow boundaries, $\mathsf{F}_{\ell,m}^{(n)}$ is made up of the incoming and the outgoing acoustic waves. By subtracting F of (3.4) from $\mathsf{F}_{\ell,m}^{(n)}$, the outgoing acoustic wave solution, F_{out}, is

$$\mathsf{F}_{\text{out}} = \mathsf{F}_{\ell,m}^{(n)} - \mathsf{F}. \tag{3.5}$$

Now F_{out}, being purely outgoing waves, must satisfy radiation boundary condition (3.1). It is to be noted that F and $\mathsf{F}_{\ell,m}^{(n)}$ and hence F_{out} are defined only on the solution mesh. To implement (3.1), the spatial and time derivatives must be discretized first. (3.1) may be rewritten in the form

$$\frac{\partial}{\partial t}\left[\mathsf{F}_{\ell,m}^{(n)} - \text{Re}\left(\hat{\mathsf{F}}\, e^{i(\alpha\ell+\beta m-\omega n\Delta t)}\right)\right] = \mathsf{W} \tag{3.6}$$

where W is

$$\mathsf{W} = -V(\theta)\left[\cos\theta\frac{\partial}{\partial x} + \sin\theta\frac{\partial}{\partial y} + \frac{1}{2r}\right]\cdot\left[\mathsf{F}_{\ell,m}^{(n)} - \text{Re}\left(\hat{\mathsf{F}}\, e^{i(\alpha\ell+\beta m-\omega n\Delta t)}\right)\right] + \text{damping terms}. \tag{3.7}$$

The discretized form of (3.6) following the DRP scheme is,

$$\mathsf{F}_{\ell,m}^{(n+1)} = \mathsf{F}_{\ell,m}^{(n)} + \Delta t\sum_{j=0}^{3} b_j\,\mathsf{W}_{\ell,m}^{(n-j)} + \text{Re}\left\{\hat{\mathsf{F}}\, e^{i(\alpha\ell+\beta m-\omega n\Delta t)}\cdot\left(e^{-i\omega\Delta t}-1\right)\right\}. \tag{3.8}$$

In the inflow boundary region (see Figure 2); i.e., the bottom three rows and the left-most three columns of mesh points, backward difference stencils are to be used to approximate the spatial derivatives of (3.7). The particular backward difference stencils to be used depend on the location of the point relative to the boundary of the computation domain. For example, for the corner point 'A' with $\ell = L$ and $m = M$ as shown in Figure 2, the discretized form of (3.7) is,

$$
\begin{aligned}
W_{L,M}^{(n)} = V(\theta_{L,M})\Bigg\{ & \cos(\theta_{L,M}) \sum_{j=-2}^{4} a_j^{24} \\
& \cdot \left[F_{L+j,M}^{(n)} - \mathrm{Re}\left(\hat{F}\, e^{i(\alpha(L+j)+\beta M-\omega n\Delta t)} \right) \right] \\
& + \sin(\theta_{L,M}) \sum_{j=-1}^{3} a_j^{15} \left[F_{L,M+j}^{(n)} \right. \\
& \left. - \mathrm{Re}\left(\hat{F}\, e^{i(\alpha L+\beta(M+j)-\omega n\Delta t)} \right) \right] \\
& + \frac{1}{2r_{L,M}} \left[F_{L,M}^{(n)} \right. \\
& \left. - \mathrm{Re}\left(\hat{F}\, e^{i(\alpha L+\beta M-\omega n\Delta t)} \right) \right] \Bigg\} \qquad (3.9) \\
& - \frac{1}{R_{\Delta x}} \Bigg\{ \sum_{j=-2}^{2} d_j^{(5)} \left[F_{L+j,M}^{(n)} \right. \\
& \left. - \mathrm{Re}\left(\hat{F}\, e^{i(\alpha(L+j)+\beta M-\omega n\Delta t)} \right) \right] \\
& + \sum_{j=-1}^{1} d_j^{(3)} \left[F_{L,M+j}^{(n)} \right. \\
& \left. - \mathrm{Re}\left(\hat{F}\, e^{i(\alpha L+\beta(M+j)-\omega n\Delta t)} \right) \right] \Bigg\}
\end{aligned}
$$

where $(r_{L,M}, \theta_{L,M})$ are the polar coordinates of the point 'A'. $d_j^{(5)}$ and $d_j^{(3)}$ are the coefficients of the 5-point and 3-point damping stencils (see Tam (1995)). Equation (3.8) supplemented by formulae for $W_{\ell,m}^{(n)}$ in the form of (3.9) is the desired nonhomogeneous radiation boundary conditions.

On the outflow boundaries, a similar treatment as above, starting with radiation boundary condition (3.3) instead of (3.1), leads to a set of inhomogeneous outflow boundary conditions.

To test whether nonhomogeneous radiation boundary conditions (3.8) and (3.9) and the corresponding outflow boundary conditions can, indeed, generate an accurate plane acoustic wave propagating across the finite computation domain without, at the same time, generating spurious vorticity or entropy waves, a series of numerical simulations have been carried out. In the simulations, a 100 × 100 mesh was used. In the interior region, time marching scheme (2.3) and (2.4) were used to time-stepping the solution to a periodic state. Along the inflow boundaries, the variables of the solution were updated using nonhomogeneous radiation boundary conditions (3.8) and (3.9). Along the outflow boundaries, nonhomogeneous outflow boundary conditions were used. Figure 3 shows the time history of convergence to the exact finite difference acoustic wave solution for the case $M = 0.5$, $\phi = 30$ deg, $\gamma = 60$ deg, $\omega = 1.2$ and $\frac{1}{R_{\Delta x}} = 0.025$. The ordinate is the maximum error; defined as the absolute value of the maximum difference (over the entire computation domain) between the numerical solution and the exact solution of the finite difference equations. The abscissa is the number of time steps. For this simulation, a zero acoustic wave initial condition was used. As can be seen, over time, the computed solution converges to the exact incoming wave solution to machine accuracy.

3.2 Incoming vorticity waves

A set of nonhomogeneous radiation and outflow boundary conditions for incoming vorticity waves can be formulated in exactly the same way as discussed above.

4. APPLICATIONS

In this section we report the results of applying the nonhomogeneous radiation and outflow boundary conditions developed in the previous section to the numerical simulation of the scattering of plane acoustic waves by a cylinder and the generation of sound by the interaction of a flat plate in a gust.

4.1 Scattering of acoustic waves by a solid cylinder

The problem of the scattering of acoustic waves by a solid cylinder was simulated numerically in the time domain. The incoming

acoustic waves were generated by the nonhomogeneous radiation boundary conditions of Section 3. A 320 × 320 mesh was used in the computation. The cylinder with a diameter of 32 was placed in the center of the computation domain. Plane acoustic waves with a wave length of 8 mesh spacings entered the computation domain from the left boundary. In the numerical simulation, the linearized Euler equations were solved using the DRP scheme. A Cartesian boundary treatment using ghost values of pressure to enforce the solid surface boundary condition of zero normal fluid velocity developed recently by Kurbatskii and Tam (1996) was applied around the surface of the cylinder. A zero acoustic wave initial condition was used to start the computation. The solution was marched in time until a time periodic state was reached.

Figure 4 shows the contours of zero pressure obtained by the numerical simulation. The zero pressure contours of the exact solution are also plotted in this figure as dotted curves. The agreement between the numerical and the exact solution is good so that the two sets of curves are almost indistinguishable. In Figure 4, the shadow zone behind the cylinder shows up prominently. There are strong scattered waves propagating backward and to the two sides of the cylinder. They are responsible for the wiggles of the zero pressure contours of the figure. The good agreement between the numerical and exact solution provides strong evidence that the proposed nonhomogeneous radiation boundary conditions are, indeed, accurate and effective.

4.2 Sound generation by the interaction of a flat plate in a gust

As another application of the nonhomogeneous radiation and outflow boundary conditions, numerical simulations of sound generation by the interaction of a flat plate in a gust (vorticity waves) were performed. The case of $M = 0.5$ and a vertical gust with

$$u = 0, \qquad v = 0.1 \sin\left[\frac{\pi}{8}\left(\frac{x}{M} - t\right)\right]$$

as shown in Figure 5 was considered. A 200 × 200 mesh was used. The flat plate had a length of 30. It was located on the x-axis in the center of the computation domain. The incoming vorticity waves were convected into the computation domain by the mean flow from the left boundary. The DRP time marching scheme was again used. The wall boundary condition on the plate was enforced by the ghost point method. Nonhomogeneous radiation boundary conditions were imposed on the left, top and bottom boundary regions. Nonhomogeneous outflow boundary conditions were imposed on the right boundary. The numerical solution was time-stepped from a zero vorticity wave initial condition until a time periodic state was established.

Figure 6 shows the computed directivity of acoustic radiation in the top half-plane. No exact solution of the present problem is available for comparison. Shown in this figure also are the computed directivities using twice and three times the original spatial resolution. It is clear from the numerical results that there is numerical convergence. This gust-plate interaction problem is a generic turbomachinery noise problem. Direct numerical simulation of this problem as a scattering problem in the time domain has never been carried out before.

5. SUMMARY

A set of nonhomogeneous radiation and outflow boundary conditions designed for use in conjunction with high-order/large-stencil finite difference schemes has been developed. The nonhomogeneous boundary conditions generate the desired incoming acoustic or vorticity waves and, at the same time, allow the scattered or internally generated disturbances to leave the computation domain with almost no reflections. These nonhomogeneous boundary conditions have been applied successfully to two benchmark aeroacoustics problems. In this work, only two-dimensional problems have been considered. The methodology, however, can easily be extended to three-dimensional problems.

ACKNOWLEDGMENT

This work was supported by NASA Langley Research Center Grant NAG 1-1776.

REFERENCES

Giles, M.B., 1990, "Non-Reflecting Boundary Conditions for Euler Equation Calculations", AIAA J., 28, 2050-2058.

Hixon, R., Shih, S.H. and Mankbadi, R.R. , 1995, "Evaluation of Boundary Con-

ditions for Computational Aeroacoustics", AIAA J., 33, 2006-2012.

Kurbatskii, K.A., and Tam, C.K.W., 1996, "Cartesian Boundary Treatment of Curved Walls for High-Order Computational Aeroacoustics Finite Difference Schemes", AIAA Paper 96-0275.

Tam, C.K.W., 1995, "Computational Aeroacoustics: Issues and Methods", AIAA Journal, 33, 1788-1796.

Tam, C.K.W. and Webb, J.C., 1993, "Dispersion-Relation-Preserving Finite Difference Schemes for Computational Acoustics", J. Comput. Phys., 107, 262-281.

Thompson, K.W., 1987, "Time Dependent Boundary Conditions for Hyperbolic Systems", J. Comput. Phys., 68, 1-24.

Thompson, K.W., 1990, "Time Dependent Boundary Conditions for Hyperbolic Systems, II", J. Comput. Phys., 89, 439-461.

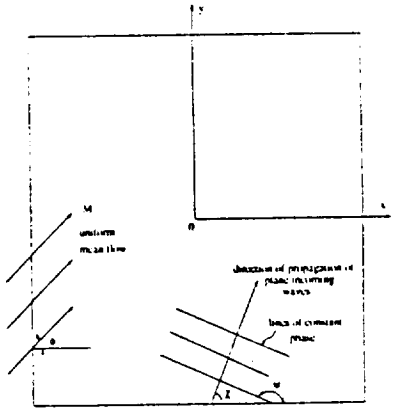

Figure 1. Computational domain showing uniform mean flow and the direction of propagation of incoming plane acoustic or vorticity waves.

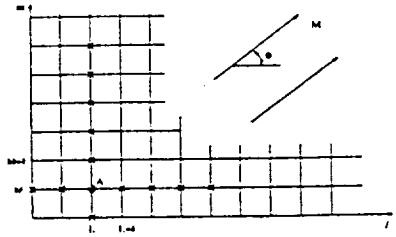

Figure 2. Backward difference stencils used to approximate spatial derivatives in the inflow boundary region of the computational domain.

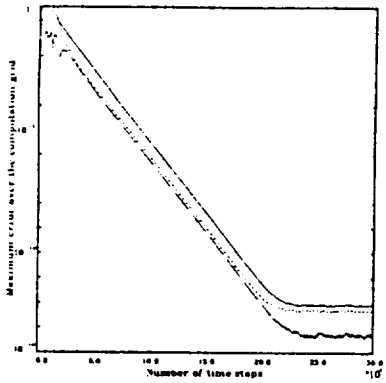

Figure 3. Convergence history of direct numerical simulation of incoming acoustic wave on a 100 x 100 grid. M=0.5, ϕ = 30 deg, χ = 60 deg, ω = 1.2, $1/R_{\Delta x} = 0.025$. ——— u, - - - - - - - v, — · — · — p.

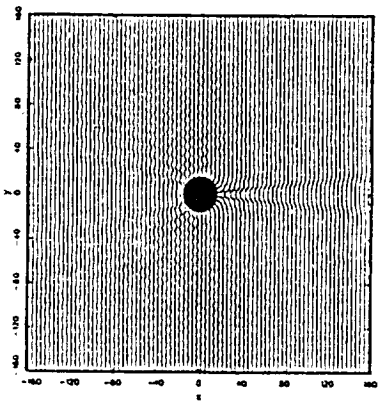

Figure 4. Map of the zero pressure contours at the beginning of a cycle associated with the scattering of plane acoustic waves by a solid cylinder. Wavelength = $8\Delta x$, Diameter of the cylinder = $32\Delta x$.

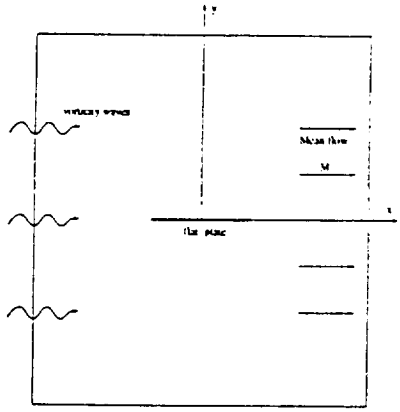

Figure 5. Schematic diagram showing the interaction of a flat plate in a vertical gust.

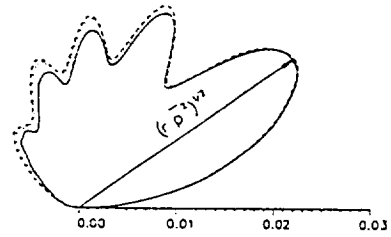

Figure 6. Directivity of sound generated by the interaction of a flat plate in a vertical gust. λ = wavelength of incoming gust. ——— $\Delta x = \lambda/8$, ... $\Delta x = \lambda/16$, - - - - - - $\Delta x = \lambda/24$.